# Core-cluster partitions of actinide nuclei

B. Buck,[1] A. C. Merchant,[1] S. M. Perez,[2,3] and H. E. Seals[2]
[1]*Department of Physics, University of Oxford, Theoretical Physics, 1 Keble Road, Oxford OX1 3NP, United Kingdom*
[2]*Department of Physics, University of Cape Town, Private Bag, Rondebosch 7700, South Africa*
[3]*iThemba LABS, P.O. Box 722, Somerset West 7129, South Africa*
(Received 1 July 2006; revised manuscript received 10 March 2007; published 20 July 2007)

We examine various techniques for assigning the core-cluster partitions of nuclei in the actinide region. The core-cluster charge products thus obtained are found to be closely correlated with the corresponding $B(E2\downarrow; 2^+ \rightarrow 0^+)$ values, with the excitation energies and with the products of valence nucleon numbers of the parent nuclei.

DOI: 10.1103/PhysRevC.76.014310 PACS number(s): 21.60.Gx, 23.20.Lv, 27.90.+b

## I. INTRODUCTION

Cluster models have a long history of application to light nuclei, predating even the discovery of the neutron [1]. Commonly, clusters of mass number $A = 3, 4$ have been very successful in the description of spectra, electromagnetic transition rates, and $\alpha$-decay widths in such nuclei. More recently, attention has shifted to heavier nuclei, where the best choice of core-cluster decomposition is open to debate. In the actinide region, $^{208}$Pb and its immediate neighbors are obvious candidates for the core of a cluster model. Indeed, many authors have combined these two ideas and successfully modeled $^{212}$Po as a $^{208}\mathrm{Pb} + \alpha$ system [2–6]. As pointed out by Tang, Wildermuth, and Pearlstein [7] in an analysis of $^6$Li as $\alpha + d$ and as $^3\mathrm{He} + {}^3\mathrm{H}$, the wave function resulting from a proper antisymmetrization of the single-nucleon wave functions in both these cluster schemes will be identical. The choice of clusterization for $^6$Li can therefore be made in terms of its convenience and ease of applicability to the property being described. We should not lose sight of this result and its implications in the actinide region. Certainly, in the heavier actinides, the choice of cluster and associated basis states may advantageously be determined by its applicability to the problem under consideration. For example, a study of $\alpha$-decay rates will be best served by using $(A-4, Z-2)+\alpha$ to describe a parent nucleus $(A, Z)$ [8,9]. Similarly, a study of exotic decay rates will be easiest when the parent nucleus is described as core + exotic cluster [3,10,11]. Nevertheless, both cluster schemes describe the same parent nucleus in its ground state, and only the sheer complexity of a 200+ particle system prevents this being shown explicitly.

### A. Buck Merchant Perez (BMP) cluster model

The model we have proposed offers the simplest possible calculation of nuclear properties because it consists of only two spinless bodies interacting through a central potential. Changes in nuclear properties from nucleus to nucleus are generated by corresponding changes in core and/or cluster so that, for example, the general decrease in level spacings and increase in $B(E2)$ strengths from the Ra to the Th, to the U, and to the Pu isotopes are generated by corresponding changes of exotic cluster from C to O, to Ne, and to Mg isotopes, respectively [10].

Alternative cluster schemes are certainly possible, but we believe them to be harder to implement than our own. Single $\alpha$ + residual core models of most actinide nuclei will require a deformed core and consideration of noncentral forces and deformed orbitals, while at least retaining the simplicity of a two-body model. Another alternative is to employ many smaller clusters in place of our single exotic cluster, with all the concomitant difficulties of the many-body problem. Such things can certainly be done, as, for example, by Cseh *et al.* [12] in their semimicroscopic algebraic model and by Schneidman *et al.* [13] in their dinuclear model. Ultimately, a detailed comparison of the predictions of these various models with experimental data will decide their usefulness.

### B. Links to collective/rotational models

A long term goal must be to demonstrate the equivalence of all these approaches or at least to find links between them. We have previously noted strong links between our cluster model and the rotational/collective model. Our calculated electromagnetic transition rates can be used to deduce equivalent shape parameters $\beta_2, \beta_3, \beta_4$, etc., for a nucleus with fixed deformation (see Table 7 of Ref. [14]). In addition, we obtain extremely similar relative motion radial wave functions for the successively higher $L$ states from this exotic cluster model. We interpret this as a manifestation, and indeed an explanation, of what is meant by "fixed intrinsic shape" [15].

The collective model's deformations are supposed to be isoscalar, which ties in exactly with the no-dipole constraint of Eq. (2) below. The continuous variability of the deformation parameters is also covered, by allowing noninteger values of the cluster charge, due to superpositions of several clusters. This allows the electromagnetic transition rates, from which the $\beta_\lambda$'s are deduced, to vary continuously. However, our cluster model is more than an alternative parametrization of the collective model, because in appropriate circumstances it produces nonrotational features. For example, in heavy nuclei it produces quasirotational spectra for heavy clusters, but not for light ones [16]. It has a common intrinsic state for high $G$, low $L \ll G$, but not for low $G$, high $L \sim G$. In our present application to a range of actinide nuclei some nonrotational features are the following: not all nuclei examined have spectra approximately proportional to $L(L+1)$, $\alpha$ and exotic

 

decay lifetimes are closely reproduced, and a cluster model interpretation of various Casten correlations [17] emerges.

### C. Core-cluster selection: The no-dipole constraint

We next turn to the choice of core and cluster in our binary cluster model. There is an important piece of experimental information that should be built into the selection procedure. The $E1$ transitions between the lowest $K^\pi = 0^+$ and $K^\pi = 0^-$ bands in actinide nuclei are very small (tiny fractions of a Weisskopf single-particle unit). This contrasts markedly with the strongly enhanced $E2$ transitions within the ground state $K^\pi = 0^+$ band (typically tens of Weisskopf units). For a core and cluster of (charge, mass) given by $(Z_1, A_1)$ and $(Z_2, A_2)$, respectively, the binary cluster model gives the reduced $E1$ transition strength for a transition from a $1^-$ to a $0^+$ state as

$$B(E1; 1^- \rightarrow 0^+) = \left[\left(\frac{Z_1}{A_1} - \frac{Z_2}{A_2}\right)\frac{A_1 A_2}{(A_1 + A_2)}\right]^2 \frac{\langle r\rangle^2}{4\pi}. \quad (1)$$

For example, treating $^{226}$Ra as a $^{222}$Rn+$\alpha$ system with $\langle r\rangle =$ 6 fm leads to a $B(E1)$ value of 0.561 e$^2$ fm$^2$ (0.234 Wu), while treating it as $^{212}$Pb + $^{14}$C with the same value for $\langle r\rangle$ leads to 0.861 e$^2$ fm$^2$ (0.360 Wu), where the Weisskopf unit is defined as $0.81A^{2/3}/4\pi$ e$^2$ fm$^2$. The measured value is 0.000645 e$^2$ fm$^2$ (0.00027 Wu). This is a typical case in the actinide region. Because the transitions are measured to be so small we deduce that, to good approximation, a no-dipole constraint,

$$\frac{Z_1}{A_1} = \frac{Z_2}{A_2} = \frac{Z_T}{A_T}, \quad (2)$$

which would make the $B(E1)$ strength vanish, is closely applicable, where $Z_T$ and $A_T$ are the total (charge, mass) with $Z_T = Z_1 + Z_2$ and $A_T = A_1 + A_2$, respectively.

This is essentially a consequence of the charge independence of the strong nuclear force. This condition can rarely be satisfied exactly by integer charge and mass values (except in the light even-even nuclei). However, fractional values of $Z_i$ can be introduced and interpreted as indicative of the need to take a linear superposition of clusters with mean charge given by the deduced fractional value of $Z_i$. This is a very important result, because it allows us to relate $A_i$ to $Z_i$, so that only one of them is independent.

### D. Core cluster selection: Previous approaches

The question of how to best describe a nucleus in terms of cluster components has been addressed (among others) by Ikeda, Takigawa, and Horiuchi [18]; Harvey [19]; Sandulescu, Poenaru, and Greiner [20]; Rae [21]; and Cseh [22]. Here, we summarize our own efforts, with special reference to a binary cluster model description of the $J^\pi = 0^+, 2^+, 4^+, \ldots$ ground state bands of even-even nuclei.

In the actinide region the observed breakup of a parent nucleus into daughter plus emitted cluster immediately suggests a possible core-cluster decomposition. Ambiguity arises because many of these nuclei decay both by exotic cluster emission and by $\alpha$-cluster emission. However, only one of these modes is consistent with the requirements of our model in which the ground state band of the parent is generated by the relative motion of a pair of spinless clusters interacting via a central potential. As an example consider the specific case of $^{232}$U, which decays both by $^{24}$Ne emission to $^{208}$Pb and by $\alpha$ emission to $^{228}$Th. For the partition into $^{208}$Pb + $^{24}$Ne there are no low-lying excited states of core or cluster below 2 MeV, and a model in which the $J^\pi = 0^+, 2^+, 4^+, \ldots$ ground state band of $^{232}$U is generated by the relative motion of a pair of spinless entities is directly applicable. This is not the case for the partition of $^{232}$U into $^{228}$Th + $\alpha$, which would require that the low-lying states of $^{228}$Th be taken into account (see Fig. 1), either by assuming that the $\alpha$ cluster moves in a deformed potential or by further subdividing $^{228}$Th into interacting spinless components that have no low-lying excited states. In column (a) of Table I, we thus list only the core cluster decompositions suggested by exotic decay as being pertinent to our present application of the model.

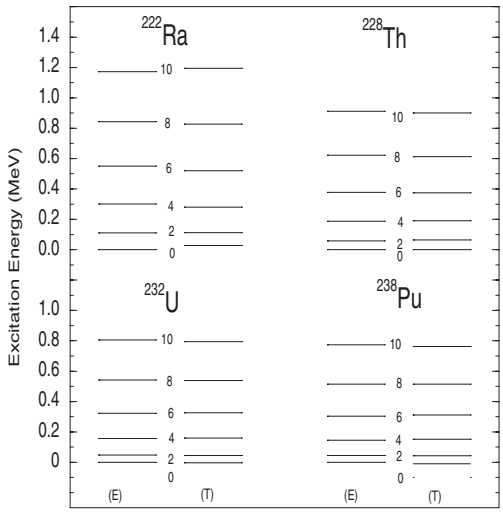


FIG. 1. Comparison of calculated (T) and experimental (E) energies for the lowest $0^+$, $2^+$, $4^+$, $6^+$, $8^+$, and $10^+$ states of $^{222}$Ra, $^{228}$Th, $^{232}$U, and $^{238}$Pu.

The above approach is only useful in the actinide region (exotic decay is not observed elsewhere) and we subsequently examined a more widely applicable stability criterion [23]. According to this criterion we generalize the strategy for locating magic numbers in nuclei and identify likely binary clusterizations by the local maxima of a function $D$ given by

$$D(Z_1, A_1, Z_2, A_2) = [B_E(Z_1, A_1) - B_L(Z_1, A_1)] + [B_E(Z_2, A_2) - B_L(Z_2, A_2)]. \quad (3)$$

In Eq. (3) $B_E$ is an actual binding energy, $B_L$ is the corresponding liquid drop value, and $(Z_1, A_1)$ and $(Z_2, A_2)$ are the core and cluster (charge, mass) respectively. $D$ is evaluated using a mixture of core-cluster partitions that satisfies the no-dipole constraint of Eq. (2). The rationale behind this method is that likely binary clusterizations should have core and cluster more tightly bound than other nearby ones, independent of the core-cluster interaction. This resulted in core cluster partitions in the actinide region consistent with those inferred from exotic decay (see columns (a) and (b) in Table I) and the technique also proved useful in cluster model applications to other parts of the periodic table [24,25]. It, however, yields poorer results for mid-shell nuclei, possibly indicating the

TABLE I. Cluster charges $Z_2$ obtained by the various methods discussed in the text (and their average values).

| Nucleus | Cluster[a] | charges[b] | $Z_2$[c] | Average $\langle Z_2 \rangle$ |
|---|---|---|---|---|
| $^{220}$Rn | – | 4.6 | 3.13 | 3.87 |
| $^{222}$Rn | – | 5.9 | 3.87 | 4.89 |
| $^{218}$Ra | – | 3.2 | 2.42 | 2.81 |
| $^{222}$Ra | 6 | 5.8 | 6.34 | 6.05 |
| $^{224}$Ra | 6 | 6.8 | 7.07 | 6.62 |
| $^{226}$Ra | 6 | 7.8 | 8.57 | 7.46 |
| $^{222}$Th | – | 5.0 | 4.05 | 4.53 |
| $^{226}$Th | – | 7.7 | 7.17 | 7.43 |
| $^{228}$Th | 8 | 8.5 | 9.47 | 8.66 |
| $^{230}$Th | 10 | 9.2 | 9.39 | 9.51 |
| $^{232}$Th | – | 9.8 | 10.86 | 10.33 |
| $^{234}$Th | – | 10.5 | 10.00 | 10.25 |
| $^{230}$U | 10 | 9.4 | 10.40 | 9.93 |
| $^{232}$U | 10 | 10.0 | 11.10 | 10.37 |
| $^{234}$U | 10.67 | 10.6 | 12.58 | 11.28 |
| $^{236}$U | – | 11.3 | 11.70 | 11.50 |
| $^{238}$U | – | 12.1 | 11.60 | 11.85 |
| $^{238}$Pu | 12.67 | 12.2 | 11.85 | 12.24 |
| $^{240}$Pu | – | 13.0 | 11.75 | 12.38 |
| $^{242}$Pu | – | 14.0 | 10.88 | 12.44 |
| $^{244}$Pu | – | 15.7 | 10.02 | 12.86 |
| $^{248}$Cm | – | 17.3 | 10.84 | 14.07 |

[a]From exotic decay.
[b]From $D$ plots.
[c]From fitting of spectra.

effects of the neglect of the core-cluster interaction or of shape changes of the core and/or cluster away from their assumed sphericity. We have thus recently investigated two further methods of assigning core-cluster partitions: one based on $B(E2)$ values [26] and the other on fitting spectra [27].

### E. Core-cluster selection: Present approach

Our principal aim in the present study is to apply the spectrum fitting method to nuclei in the actinide region, where the core-cluster partitions inferred from exotic decay and from applications of the maximum stability criterion provide useful consistency checks.

## II. CORE-CLUSTER PARTITIONS

In the analysis we include all heavy even-even nuclei with total proton and neutron numbers $Z_T \geqslant 86$ and $N_T \geqslant 130$, respectively, for which the excitation energies of the $J^\pi = 0^+, 2^+, \ldots, 10^+$ states of the ground state bands, as well as the corresponding $B(E2)$ values, are known. We list these nuclei in Table I, together with the cluster charges $Z_2$ inferred from the various partition methods discussed in Sec. I D above. So, for example, wherever exotic decay was observed we assigned a value of $Z_2$ corresponding to the emitted cluster charge (or average thereof, if more than one kind of exotic cluster was found to be emitted). Table I also lists $Z_2$ values deduced from the maximum stability criterion [23].

Core-cluster partitions can also be obtained by optimizing cluster model fits to spectra [27], using a core-cluster interaction $V(r) = V_N(r) + V_C(r)$ with a nuclear component $V_N(r)$ given by

$$V_N(r) = v_a A_2 \left[ \frac{x}{\{1 + \exp[(r - R)/a]\}} + \frac{1 - x}{\{1 + \exp[(r - R)/3a]\}^3} \right] \quad (4)$$

and a Coulomb component $V_C(r)$ of standard form [27]. We have previously found that setting

$$v_a = 55.7 \text{ MeV}, \quad a = 0.75 \text{ fm}, \quad x = 0.36, \quad (5)$$

a global quantum number $G = 5A_2$, and a radius parameter $R$ fitted to the appropriate exotic decay $Q$ value results in excellent fits to the observed exotic decay widths [28], with a goodness-of-fit indicator $S = 169$ corresponding to agreement between theory and experiment at the level of a factor of two. We note that the asymptotic form of $V_N(r)$, important in determining these decay widths, is weakly dependent on the mixing parameter $x$. We accordingly find that setting

$$v_a = 58.1 \text{ MeV}, \quad a = 0.75 \text{ fm}, \quad x = 0.30, \quad G = 5A_2 \quad (6)$$

preserves the good fits to the exotic decay data (with a goodness-of-fit indicator $S = 173$) while at the same time improving the overall agreement between the core-cluster partitions obtained by the spectrum fitting technique with those obtained by the other methods discussed above. We thus use a nuclear potential $V_N(r)$ defined by Eqs. (4) and (6) in determining the core-cluster partitions by the spectrum fitting technique [27]. The results are summarized in Table II, with typical examples of the excellent fits obtained to the spectra shown in Fig. 1.

The cluster charges generated by the various methods are compared in Table I. We note the good overall agreement with the exception of nuclei in the very heavy region with $A_T > 240$. The problem is a deviation from the systematics relating the excitation energy of the $2^+$ first excited state to its $B(\text{E2}\downarrow; 2^+ \rightarrow 0^+)$ transition strength. Broadly speaking, it has been known since the time of Grodzins [29] that, as the excitation energy falls, the $B(E2)$ strength increases for nuclei within isotopic sequences (with some slight dependence on mass also). The precise functional form of this dependence continues to be debated [30], but the general trend is sufficiently well established for it to be used as a predictive tool for unknown $B(E2)$'s when the $2^+$ energy is known [31]. In $^{242}$Pu, $^{244}$Pu, and $^{248}$Cm the $B(E2)$ strength to $2^+$ energy correlation is not obeyed by the data. This is not predicted by our model and, rather than speculate on the causes of this anomaly with inadequate information, we omit these nuclei from further analysis.

## III. CORRELATIONS

The cluster model predicts a number of relations between the core-cluster charge products $Z_1 Z_2 / Z_T$ obtained above and other quantities of interest [32]. The model expression for

TABLE II. Cluster charges, masses, and potential radii from optimal cluster model fits to spectra (see text for discussion).

| Nucleus | Cluster ($Z_2$, $A_2$) | $R$ (fm) |
|---|---|---|
| $^{220}$Rn | (3.13, 8.0) | 6.842 |
| $^{222}$Rn | (3.87, 10.0) | 6.723 |
| $^{218}$Ra | (2.42, 6.0) | 6.873 |
| $^{222}$Ra | (6.34, 16.0) | 6.649 |
| $^{224}$Ra | (7.07, 18.0) | 6.644 |
| $^{226}$Ra | (8.57, 22.0) | 6.604 |
| $^{222}$Th | (4.05, 10.0) | 6.775 |
| $^{226}$Th | (7.17, 18.0) | 6.657 |
| $^{228}$Th | (9.47, 24.0) | 6.618 |
| $^{230}$Th | (9.39, 24.0) | 6.606 |
| $^{232}$Th | (10.86, 28.0) | 6.621 |
| $^{234}$Th | (10.00, 26.0) | 6.585 |
| $^{230}$U | (10.40, 26.0) | 6.585 |
| $^{232}$U | (11.10, 28.0) | 6.643 |
| $^{234}$U | (12.58, 32.0) | 6.649 |
| $^{236}$U | (11.70, 30.0) | 6.626 |
| $^{238}$U | (11.60, 30.0) | 6.620 |
| $^{238}$Pu | (11.85, 30.0) | 6.632 |
| $^{240}$Pu | (11.75, 30.0) | 6.643 |
| $^{242}$Pu | (10.88, 28.0) | 6.666 |
| $^{244}$Pu | (10.02, 26.0) | 6.663 |
| $^{248}$Cm | (10.84, 28.0) | 6.700 |

$B(E2; 2^+ \to 0^+)$ is given by

$$B(E2) = \frac{1}{4\pi}\left\{\frac{Z_1 Z_2}{Z_T}\int \chi_2(r) r^2 \chi_0(r)\, dr\right\}^2, \tag{7}$$

where $\chi_\lambda(r)$ is the radial wave function of the core-cluster relative motion for angular momentum $\lambda$. For near-identical $\chi_\lambda(r)$ [33] we can then write

$$\begin{aligned} B(E2) &\sim \frac{1}{4\pi}\left\{\frac{Z_1 Z_2}{Z_T}\int \chi_0^2(r) r^2\, dr\right\}^2 \\ &\sim \frac{1}{4\pi}\left\{\frac{Z_1 Z_2}{Z_T} r_0^2 A_T^{2/3}\right\}^2, \\ \text{i.e.,}\ \frac{\sqrt{B(E2)}}{A_T^{2/3}} &= \frac{1}{\sqrt{4\pi}} r_0^2 \left\{\frac{Z_1 Z_2}{Z_T}\right\}. \end{aligned} \tag{8}$$

We now seek a relation between excitation energy differences and $Z_1 Z_2/Z_T$. The radial Schrödinger equation for $\chi_\lambda(r)$ reads

$$\frac{-\hbar^2}{2\mu}\frac{d^2\chi_\lambda}{dr^2} + V(r)\chi_\lambda + \frac{\hbar^2\lambda(\lambda+1)}{2\mu r^2}\chi_\lambda = E_\lambda \chi_\lambda, \tag{9}$$

where $V(r)$ is the core-cluster potential and $\mu = A_1 A_2/A_T$ is the reduced mass.

Premultiplying Eq. (9) for $\lambda = \ell$ by the solution $\chi_L(r)$ for $\lambda = L$, subtracting the resulting expression from the corresponding one with $\ell$ and $L$ interchanged, and integrating over the radial coordinate yields

$$\frac{1}{(E_L - E_\ell)} = \frac{\mu I_{L\ell}}{d_{L\ell}}, \tag{10}$$

where

$$d_{L\ell} = \frac{\hbar^2}{2}\{L(L+1) - \ell(\ell+1)\} \tag{11}$$

and

$$I_{L\ell} = \left[\int \chi_L(r)\frac{1}{r^2}\chi_\ell(r)\, dr\right]^{-1} \int \chi_L(r)\chi_\ell(r)\, dr. \tag{12}$$

The $I_{L\ell}$ may be rewritten

$$I_{L\ell} \sim r_{L\ell}^2 A_T^{2/3}, \tag{13}$$

where, under the assumption of near-identical $\chi_\lambda(r)$, we expect the $r_{L\ell}$ to be similar to each other. Finally, making use of the no-dipole rule of Eq. (2) we can write

$$\mu = \frac{A_1 A_2}{A_T} = \frac{Z_1 Z_2}{Z_T}\frac{A_T}{Z_T}, \tag{14}$$

so that

$$\left\{\frac{Z_T}{(E_L - E_\ell)A_T^{5/3}}\right\} = \frac{1}{d_{L\ell}} r_{L\ell}^2 \frac{Z_1 Z_2}{Z_T}. \tag{15}$$

As in a previous analysis [32] we concentrate on $L = 2$, $\ell = 0$ and $L = 4$, $\ell = 2$ here.

We can also relate the charge products $Z_1 Z_2/Z_T$ to the products $N_P N_N$, which occur in various forms of the Casten correlations [17]. Here $N_P$ and $N_N$ are the number of valence protons and valence neutrons, respectively. For the simplest case of a near-magic core, so that the cluster has $Z_2 \sim Z_P$ and $N_2 \sim N_N$, and small cluster, so that the core has $Z_1 \sim Z_T$ and $N_1 \sim N_T$, we have, using the no-dipole rule of Eq. (2),

$$N_P N_N = Z_2 N_2 = Z_2^2 \frac{N_T}{Z_T} \approx \left(\frac{Z_1 Z_2}{Z_T}\right)^2 \frac{N_T}{Z_T}, \tag{16}$$

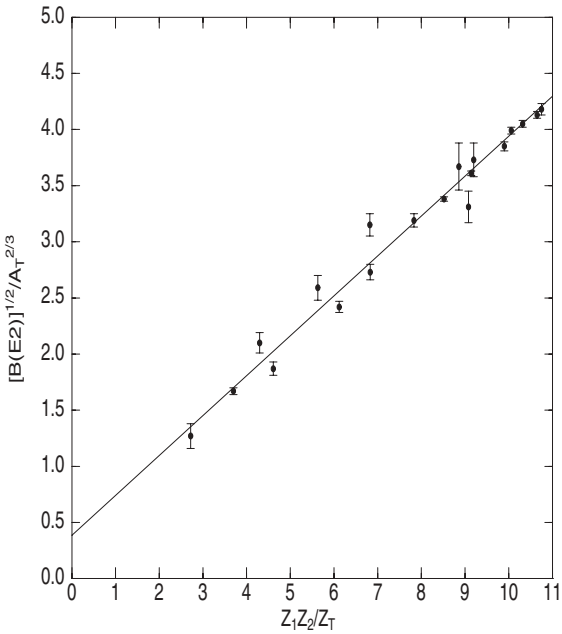


FIG. 2. Plot of measured values of $[B(E2 \text{ in e}^2\text{ fm}^4)]^{1/2}/A_T^{2/3}$, with error bars [31], against $Z_1 Z_2/Z_T$, where the deduced cluster charges are taken from Table I. The best straight line fit (solid line) has a gradient of $0.3555 \pm 0.0132$ and a $y$ intercept of $0.3858 \pm 0.1060$.

so that

$$\sqrt{\frac{Z_T}{N_T}}\{N_P N_N\}^{1/2} = \left\{\frac{Z_1 Z_2}{Z_T}\right\}. \quad (17)$$

For the actinide region analyzed here, $N_P$ and $N_N$ are calculated using the standard shell closures at $Z = 82$ and $N = 126$, respectively.

We note that a number of assumptions have been made in deriving Eqs. (8), (15), and (17), and in particular that of near-identical radial wave functions $\chi_\lambda(r)$. We thus replace these relations by the less restrictive forms

$$\frac{\sqrt{B(E2)}}{A_T^{2/3}} = a_0 + \frac{1}{\sqrt{4\pi}} r_0^2 \left\{\frac{Z_1 Z_2}{Z_T}\right\}, \quad (18)$$

$$\left\{\frac{Z_T}{(E_L - E_\ell)A_T^{5/3}}\right\} = a_{L\ell} + \frac{r_{L\ell}^2}{d_{L\ell}} \left\{\frac{Z_1 Z_2}{Z_T}\right\}, \quad (19)$$

and

$$\sqrt{\frac{Z_T}{N_T}}\{N_P N_N\}^{1/2} = \alpha + \beta \left\{\frac{Z_1 Z_2}{Z_T}\right\}. \quad (20)$$

We have applied Eqs. (18)–(20) to the present data for $A_T \leqslant 240$, using the averaged $Z_2$ values from Table I. Figure 2 shows a plot of Eq. (10), together with a linear fit corresponding to $a_0 = 0.39 \pm 0.11$ and $r_0 = 1.12 \pm 0.02$ fm. We note that these values are in good accord with expectation and strongly support the overall consistency of the analysis. Plots of Eq. (19) with $L = 2, \ell = 0$ and $L = 4, \ell = 2$ are shown in Figs. 3 and 4, respectively. The linear fits result in

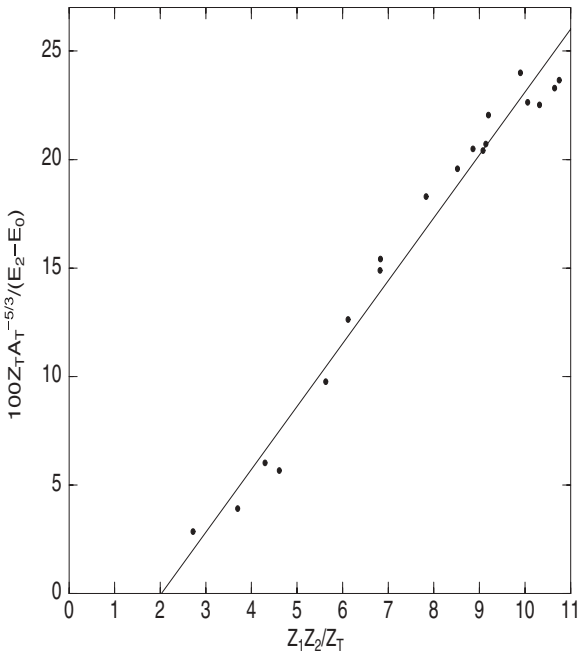


FIG. 3. Plot of $100 Z_T A_T^{-5/3}/(E_2 - E_0)$ against $Z_1 Z_2/Z_T$, where the measured excitation energies in MeV are taken from the appropriate Nuclear Data Sheets and the cluster charges are taken from Table I. The best straight line fit (solid line) has a gradient of $2.8975 \pm 0.1062$ and a $y$ intercept of $-5.8663 \pm 0.8508$.

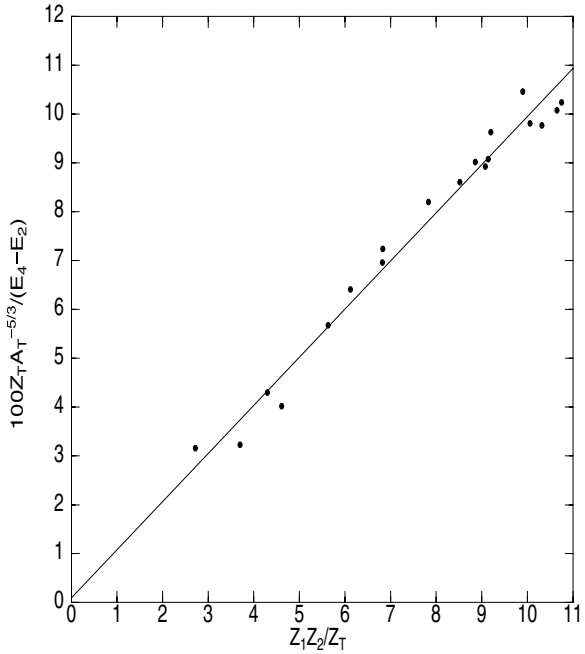


FIG. 4. Plot of $100 Z_T A_T^{-5/3}/(E_4 - E_2)$ against $Z_1 Z_2/Z_T$, where the measured excitation energies in MeV are taken from the appropriate Nuclear Data Sheets and the cluster charges are taken from Table I. The best straight line fit (solid line) has a gradient of $0.9860 \pm 0.0351$ and a $y$ intercept of $0.0958 \pm 0.2813$.

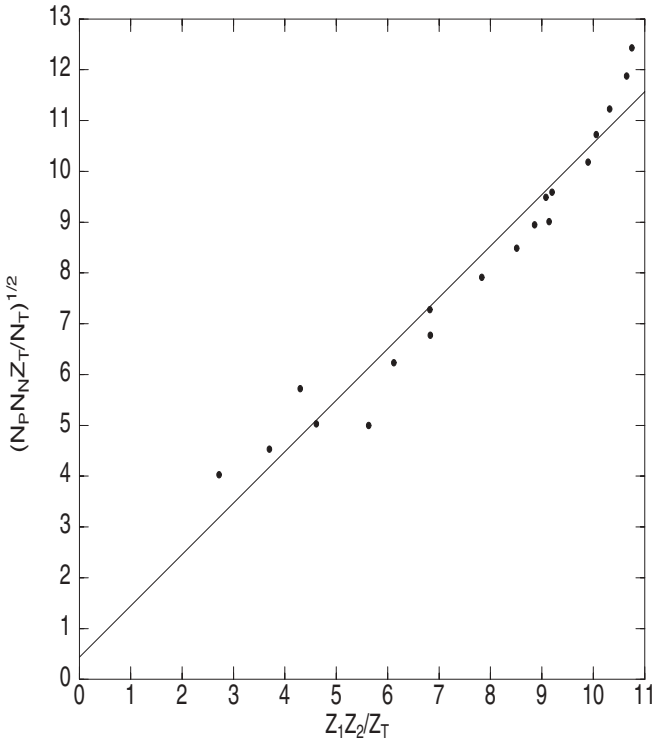


FIG. 5. Plot of $(N_P N_N Z_T/N_T)^{1/2}$ against $Z_1 Z_2/Z_T$, where $N_P$ and $N_N$ are the valence proton and neutron numbers, respectively, and the cluster charges are taken from Table I. The best straight line fit (solid line) has a gradient of $1.0113 \pm 0.0516$ and a $y$ intercept of $0.4408 \pm 0.4129$.

$a_{20} = (-5.87 \pm 0.85) \times 10^{-2}$ and $r_{20} = 1.91 \pm 0.02$ fm and $a_{42} = (0.096 \pm 0.28) \times 10^{-2}$ and $r_{42} = 1.70 \pm 0.03$ fm, respectively.

An early finding [34] regarding applications of the cluster model is that $\ell = 0$ ground states tend to be underbound with respect to the rest of the spectrum. This results in the $L = 2$ to $\ell = 0$ energy difference being less well reproduced in the model than all the other energy differences in the spectrum, particularly for light clusters in heavy nuclei. Removing the points corresponding to clusters with $Z_2 \leqslant 6.0$ from Fig. 3 results in $a_{20} = (-1.11 \pm 1.31) \times 10^{-2}$ and $r_{20} = 1.73 \pm 0.05$ fm, with the values of $a_{20}$ and $a_{42}$ consistent with zero and the values of $r_{20}$ and $r_{42}$ consistent with each other. We note here that the values of $r_0$, $r_{20}$, and $r_{42}$ thus obtained give valuable direct information on matrix elements of $r^2$ and $1/r^2$, and hence on the underlying radial wave functions $\chi_\lambda(r)$.

Finally, Fig. 5 shows the results of plotting Eq. (20) with the fitted line corresponding to $\alpha = 0.44 \pm 0.41$ and $\beta = 1.01 \pm 0.05$, in excellent agreement with the values $\alpha = 0$ and $\beta = 1.0$ expected from Eq. (17). We note that this is fundamental to a cluster model interpretation [32] of Casten-type correlations [17], for it then follows that substituting $\sqrt{N_P N_N Z_T / N_T}$ for $Z_1 Z_2 / Z_T$ in Eqs. (18) and (19) generates linear plots similar to those of Figs. 2, 3, and 4.

## IV. CONCLUSIONS

We have generated the core-cluster charge products $Z_1 Z_2 / Z_T$ for an extensive set of even-even nuclei in the actinide region, by fitting the spectra of their ground state bands. The core-cluster charge products thus obtained are consistent with values generated by other methods. As predicted by a binary cluster model, the $Z_1 Z_2 / Z_T$ values are found to be closely correlated with expressions involving the $B(E2)$ values, excitation energies, and products of valence nucleon numbers. This provides strong support for the applicability of the model in this mass region, as well as for a cluster model interpretation of the Casten correlations.


[1] G. Gamow, Proc. R. Soc. London A **126**, 632 (1930).
[2] K. Varga, R. G. Lovas, and R. J. Liotta, Nucl. Phys. **A550**, 421 (1992).
[3] B. Buck and A. C. Merchant, Phys. Rev. C **39**, 2097 (1989).
[4] B. Buck, A. C. Merchant, and S. M. Perez, Phys. Rev. Lett. **72**, 1326 (1994).
[5] S. Ohkubo, Phys. Rev. Lett. **74**, 2176 (1995).
[6] F. Hoyler, P. Mohr, and G. Staudt, Phys. Rev. C **50**, 2631 (1994).
[7] Y. C. Tang, K. Wildermuth, and L. D. Pearlstein, Nucl. Phys. **32**, 504 (1962); K. Wildermuth and Y. C. Tang, *A Unified Theory of the Nucleus* (Academic Press, New York, 1977), p. 23.
[8] B. Buck, A. C. Merchant, and S. M. Perez, J. Phys. G **17**, 1223 (1991).
[9] B. Buck, A. C. Merchant, and S. M. Perez, J. Phys. G **18**, 143 (1992).
[10] B. Buck, A. C. Merchant, and S. M. Perez, Phys. Rev. Lett. **76**, 380 (1996).
[11] B. Buck, A. C. Merchant, S. M. Perez, and P. Tripe, J. Phys. G **20**, 352 (1994).
[12] J. Cseh, A. Algora, J. Darai, and P. O. Hess, Phys. Rev. C **70**, 034311 (2004).
[13] T. M. Schneidman, G. G. Adamian, N. V. Antonenko, R. V. Jolos, and W. Scheid, Phys. Rev. C **67**, 014313 (2003).
[14] B. Buck, A. C. Merchant, and S. M. Perez, Nucl. Phys. **A617**, 195 (1997).
[15] B. Buck, A. C. Merchant, and S. M. Perez, Phys. Rev. C **57**, R2095 (1998).
[16] B. Buck, A. C. Merchant, and S. M. Perez, J. Phys. G **38**, 65 (2004).
[17] R. F. Casten and N. V. Zamfir, J. Phys. G **22**, 1521 (1996).
[18] K. Ikeda, N. Takigawa, and H. Horiuchi, Suppl. Prog. Theor. Phys. Extra Number 464 (1968).
[19] M. Harvey in *Proceedings of the 2nd International Conference on Clustering Phenomena in Nuclei, College Park, Maryland 1975,* USDERA Report No. ORO–4856–26, p. 549.
[20] A. Sandulescu, D. N. Poenaru, and W. Greiner, Sov. J. Part. Nuclei **11**, 528 (1980).
[21] W. D. M. Rae, Int. J. Mod. Phys. A **3**, 1343 (1988).
[22] J. Cseh, J. Phys. G **19**, L97 (1993).
[23] B. Buck, A. C. Merchant, M. J. Horner, and S. M. Perez, Phys. Rev. C **61**, 024314 (2000).
[24] B. Buck, A. C. Merchant, and S. M. Perez, Nucl. Phys. **A652**, 211 (1999); **A657**, 267 (1999).
[25] B. Buck, A. C. Merchant, and S. M. Perez, Phys. Rev. C **61**, 014310 (1999).
[26] B. Buck, A. C. Merchant, V. A. McBride, and S. M. Perez, J. Phys. G **30**, 1371 (2004).
[27] B. Buck, A. C. Merchant, and S. M. Perez, Phys. Rev. C **71**, 014311 (2005).
[28] B. Buck, A. C. Merchant, S. M. Perez, and H. E. Seals, J. Phys. G **31**, 1499 (2005).
[29] L. Grodzins, Phys. Lett. **2**, 88 (1962).
[30] B. Buck, A. C. Merchant, V. A. McBride, and S. M. Perez, Phys. Rev. C **66**, 067303 (2002).
[31] S. Raman, C. W. Nestor, Jr., S. Kahane, and K. H. Bhatt, At. Data Nucl. Data Tables **42**, 1 (1989).
[32] B. Buck, A. C. Merchant, and S. M. Perez, Phys. Rev. Lett. **94**, 202501 (2005).
[33] B. Buck, A. C. Merchant, and S. M. Perez, Phys. Rev. C **59**, 750 (1999).
[34] B. Buck, A. C. Merchant, and S. M. Perez, Phys. Rev. C **51**, 559 (1995).